

Cosmic rays cannot explain the high ionisation rates in the Galactic centre

S. Ravikularaman¹, S. Recchia², V. H. M. Phan³ and S. Gabici¹

¹ Université Paris Cité, CNRS, Astroparticule et Cosmologie, F-75013 Paris, France
e-mail: ravikularaman@apc.in2p3.fr

² INAF-Osservatorio Astronomico di Brera, Via Bianchi 46, I-23807 Merate, Italy

³ Sorbonne Université, Observatoire de Paris, PSL Research University, LERMA, CNRS UMR 8112, 75005 Paris, France

January 17, 2025

ABSTRACT

Context. The H₂ ionisation rate in the central molecular zone, located in the Galactic centre, is estimated to be $\zeta \sim 2 \times 10^{-14} \text{ s}^{-1}$, based on observations of H₃⁺ lines. This value is two to three orders of magnitude larger than that measured anywhere else in the Galaxy.

Aims. Due to the high density of the gas in the central molecular zone, UV and X-ray photons do not penetrate this region. Hence, cosmic rays are expected to be the exclusive agents of ionisation. A high cosmic-ray density has been invoked to explain the unusually high ionisation rate. However, this excess is not seen in the γ -ray emission from this region, which is produced by high-energy cosmic rays. Therefore, an excess is expected only in the low-energy cosmic-ray spectrum. Here, we derive constraints on this hypothetical low-energy component in the cosmic-ray spectra, and we question its plausibility.

Methods. To do so, we numerically solved the cosmic-ray transport equation in the central molecular zone, considering spatial diffusion, advection in the Galactic wind, re-acceleration in the ambient turbulence, and energy losses due to interactions with matter and radiation in the interstellar medium. We derived stationary solutions under the assumption that cosmic rays are continuously injected by a source located in the Galactic centre. The high-energy component in the cosmic-ray spectrum was then fitted to available γ -ray and radio data, and a steep low-energy component was added to the cosmic-ray spectrum to explain the large ionisation rates.

Results. We find that injection spectra of p^{-7} for protons below $p_{\text{enh},p}c \approx 780 \text{ MeV}$ and $p^{-5.2}$ for electrons below $p_{\text{enh},e}c = 1.5 \text{ GeV}$ are needed to reach the observed ionisation rates. This corresponds to a cosmic-ray power of the order of $\sim 10^{40-41} \text{ erg s}^{-1}$ injected at the Galactic centre. Not only is this unrealistic, but it is also impossible to reproduce a constant ionisation rate across the region, as observations suggest.

Conclusions. We conclude that cosmic rays alone cannot explain the high ionisation rates in the Galactic centre.

Key words. Galaxy: center – ISM: cosmic rays – Gamma rays: ISM – Radio continuum: ISM – Radiation mechanisms: non-thermal – ISM: clouds

1. Introduction

At the centre of the Milky Way, located $\sim 8.5 \text{ kpc}$ from the Solar System, lies the supermassive black hole (SMBH) Sagittarius A* (Sgr A*). It is surrounded by the Galaxy's densest and most massive molecular clouds (MCs), forming an asymmetric ring-like structure of molecular hydrogen gas (Ferrière et al. 2007). This region is named the central molecular zone (CMZ) and occupies a roughly cylindrical volume that has a radius of $\approx 200 \text{ pc}$ and a height of $\approx 100 \text{ pc}$.

The star formation rate in the CMZ is $\approx 0.07^{+0.08}_{-0.02} M_{\odot} \text{ yr}^{-1}$, a number significantly lower than expected given the amount of dense gas in this region (Henshaw et al. 2023). Hence, it is vital to understand the process and requirements for star formation in this region. One of the critical ingredients for star formation is the gas ionisation rate, which measures the number of ionisations an atom or a molecule of hydrogen undergoes per unit of time. A few different definitions exist for this quantity (Neufeld & Wolfire 2017). In this paper, we refer to the ionisation rate as the production rate of H₂⁺ ions per hydrogen molecule.

The ionisation potential of H₂ is $I = 15.426 \text{ eV}$. Both cosmic rays (CRs) and photons (UV, X-rays) can ionise H₂:



but it is believed that the first reaction largely dominates the second one in MCs, as ionising photons cannot penetrate large column densities of gas (McKee 1989). Among CRs, those with particle energy in the sub-giga-electronvolt domain are believed to be most effective in ionising interstellar matter (see e.g. Gabici 2022, and references therein).

The ionisation of molecular hydrogen is followed by the extremely rapid ion-neutral reaction (Oka 2006):



leading to the production of H₃⁺ ions. Other ionisation processes, such as double or dissociative ionisation, are negligible compared to these processes (Padovani et al. 2009) and will be ignored in the following.

H₃⁺ is destroyed through dissociative recombination, according to one of the two following reactions (Oka 2006):



The rate of H_3^+ destruction through recombination per unit volume is

$$r_{\text{des}}^{\text{H}_3^+} = k_e n(\text{H}_3^+) n(e^-), \quad (6)$$

where k_e is the Langevin rate constant for this reaction determined in laboratory experiments (McCall et al. 2003). For typical cloud temperatures of a few tens of degrees, $k_e \approx 10^{-7} \text{ cm}^3 \text{ s}^{-1}$. By balancing the rates of formation and destruction of H_3^+ , we obtain an expression for the ionisation rate:

$$\zeta_{\text{CR}}^{\text{H}_3} = \frac{2k_e x_e}{f_{\text{H}_2}} \frac{N(\text{H}_3^+)}{L}, \quad (7)$$

where x_e is the electron fraction, $f_{\text{H}_2} = 2n(\text{H}_2)/n_{\text{H}}$ is the fraction of molecular hydrogen, and $N(\text{H}_3^+)$ is the H_3^+ column density along the line of sight of length L . The latter quantity is the most uncertain and is usually estimated by assuming that clouds are roughly spherical. The other quantities on the right side of the equation can be constrained from observations (see e.g. McCall et al. 2003, and references therein for the case of a diffuse cloud towards ζ Persei).

The ionisation rate in the local interstellar medium, measured by Voyager I, has been found to be in the range of $1.51 - 1.64 \times 10^{-17} \text{ s}^{-1}$ (Cummings et al. 2016). Observations towards various lines of sight in the Galaxy have shown that the ionisation rate is of the order of $\approx 10^{-16} \text{ s}^{-1}$ in diffuse clouds and $\approx 10^{-17} \text{ s}^{-1}$ in dense clouds, with a quite large dispersion around these values (Caselli et al. 1998; Indriolo & McCall 2012; Padovani et al. 2009; Phan et al. 2018). These values are much larger (by a factor of 10 to 100) than expected if one makes the assumption that the CR intensity changes only very mildly across the Galaxy (Phan et al. 2018). A possible solution to this puzzle is to assume that, in fact, the intensity of low-energy (ionising) CRs varies spatially, and is larger close to CR accelerators (Phan et al. 2021, 2023).

The discrepancy is even more striking in the region very close to the Galactic centre (GC). By analysing the absorption spectra of various stars, Oka et al. (2005) measured the H_3^+ column density and concluded that the ionisation rate in the CMZ is $(2 - 7) \times 10^{-15} \text{ s}^{-1}$. Based on new sight lines from Geballe & Oka (2010), Goto et al. (2011) concluded that the ionisation rates in the CMZ were $> 10^{-15} \text{ s}^{-1}$, which was later corroborated by other infrared observations (Goto et al. 2014). Le Petit et al. (2016) question the validity of the linear relation between $N(\text{H}_3^+)$ and ζ and suggest that it only holds up to a certain value of the ionisation rate. Using the Meudon photon-dominated region (PDR) code (Le Petit et al. 2006), they found that the ionisation rate in the GC must be $1 - 11 \times 10^{-14} \text{ s}^{-1}$. This value is in accordance with Oka et al. (2019)'s most recent analysis of 30 stellar spectra, in which they raise their initial estimate by an order of magnitude to $\zeta_{\text{CMZ}} = 2 \times 10^{-14} \text{ s}^{-1}$.

Yusef-Zadeh et al. (2007) used another method to constrain the ionisation rate. They analysed γ -rays, radio synchrotron emissions, and the Iron $K\alpha$ line and concluded that along certain lines of sight the ionisation rate could be as high as $5 \times 10^{-13} \text{ s}^{-1}$. Later, they reduced this upper limit to 10^{-14} s^{-1} (Yusef-Zadeh et al. 2013).

Molecules like H_3O^+ are produced in MCs as the result of chemical reaction chains initiated by the ionisation of molecular

hydrogen. These molecules have also been used to constrain the ionisation rate in the vicinity of the GC. In particular, van der Tak et al. (2006) analysed H_3O^+ maps of the Sgr B2 region and found that an ionisation rate of $4 \times 10^{-16} \text{ s}^{-1}$ reproduced the $\text{H}_3\text{O}^+/\text{H}_2\text{O}$ ratio in the cloud envelope. Although this value is lower than early estimates, a more recent Herschel survey of H_3O^+ suggests higher ionisation rates of $> 10^{-15} \text{ s}^{-1}$ (Indriolo et al. 2015).

Most recently, observations of other molecules have also hinted at a high ionisation rate. Ginsburg et al. (2016) observed the $J = 3 - 2$ transition of para-formaldehyde (p- H_2CO) to estimate the gas temperature of the CMZ and set the upper limit for the ionisation rate as 10^{-14} s^{-1} . The measured abundances of PO^+ (Rivilla et al. 2022) and HCOS^+ (Sanz-Novo et al. 2024) towards the G+0.693–0.027 MC in the CMZ also imply an ionisation rate of $10^{-15} - 10^{-14} \text{ s}^{-1}$.

The values of the ionisation rate measured in the CMZ employing various techniques range, then, from $\approx 10^{-15}$ to $\approx 10^{-13} \text{ s}^{-1}$, which are much larger (by up to few orders of magnitude) than the values measured from diffuse and dense clouds in the Galaxy. Although an increase in the CR density, and therefore in the CR ionisation rate, might be expected towards the centre of the Galaxy, the increase is predicted to be at most a few factors (see e.g. Wolfire et al. 2003). It follows that, in order to explain the extremely large ionisation rates seen in the CMZ, one should invoke an equally large excess in sub-giga-electronvolt CRs there, and that this excess is due to a new component in the CR spectrum that is unrelated to the CR background that pervades the entire Galaxy.

This is even more puzzling, as tracers of the spatial distribution of higher-energy (giga-electronvolt) CRs in the Galaxy, such as γ -rays produced in CR interactions with interstellar matter, do not reveal the presence of a significant excess in the CMZ (see e.g. Fig. 9 in Gabici 2022, and references therein). This implies that a large excess must only be present in low-energy CRs.

Remarkably, the H.E.S.S. Collaboration reported on the detection of the CMZ in tera-electronvolt γ -rays. The spatial morphology of the emission indicates that a source of CRs has to be present in the vicinity of Sgr A* and that such a source is most probably a continuous injector of CRs (HESS Collaboration et al. 2016). The excess in multi-tera-electronvolt CRs derived from such measurements is several factors, and indicates that a new component in the spectrum of high-energy CRs is indeed present in the CMZ.

In this paper, we study whether it is possible for CRs to cause the very large ionisation rates observed in the CMZ. In particular, we assume that a CR accelerator is present in the vicinity of the GC and that such an accelerator injects particles continuously into the CMZ. Our goal is to constrain the spectral energy distribution and the rate at which CRs have to be injected in order to explain the measured ionisation rates. We conclude that the power requirement to fit data is exceedingly large, and therefore the cause of the large ionisation rate has to be searched for elsewhere.

In the next section, we describe the model for CR transport in the CMZ, including all the fiducial parameters. In Sec.3 and 4, we constrain the high-energy CR proton and electron spectra from diffuse γ -ray and radio observations of the CMZ, respectively. We extrapolate these high-energy spectra to lower energies and compute the ionisation rates in Sec.5. As these values are smaller by several orders of magnitude than the measured ionisation rates in the CMZ, we add a steep power-law component in the injection spectrum of CRs, and we try steeper and steeper slopes until the predicted ionisation rates reach the observed values. After studying the spatial variation in this value

across the entire CMZ, we discuss the uncertainty introduced by the unknown depth, L , into the CMZ of the stars used for H_3^+ absorption measurements. Most importantly, we compute the power W_{CR} of CRs and their energy density, n_{CR} , needed to explain the measurements of the ionisation rate. We show in Sec.6 that the CR spectra suitable to reproduce the large ionisation rates contradict other observations of the CMZ, and we eventually conclude that CRs cannot explain the large ionisation rates (Sec.7).

2. Cosmic-ray transport in the central molecular zone

The CMZ was modelled as a cylinder of uniform gas density, n_{CMZ} . The cylinder has a radius of $R_{\text{CMZ}} \sim 200$ pc (Ferrière et al. 2007) and height of $H_{\text{CMZ}} \sim 100$ pc, and is centred around Sgr A* at $D_{\text{GC}} \sim 8.5$ kpc (see Fig. 1). The gas mass of the CMZ has been estimated to be $M_{\text{CMZ}} \sim 6 \times 10^7 M_{\odot}$ (Dahmen et al. 1998; Tsuboi et al. 1999), which implies that the average gas density is $n_{\text{CMZ}} = 1.5 \times 10^2 \text{ cm}^{-3}$. The CMZ is embedded in the Galaxy's gaseous disc, which is assumed to have the same height as the CMZ, H_{CMZ} , and characterised by a gas density of $n_{\text{disk}} \sim 1 \text{ cm}^{-3}$. Outside of the Galactic disc, the gas density was set equal to $n_{\text{out}} \sim 10^{-2} \text{ cm}^{-3}$, which is appropriate to describe the Galactic halo.

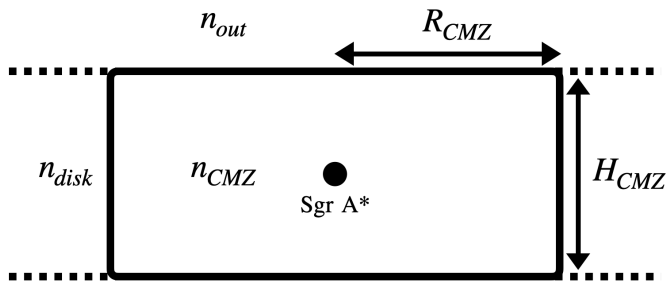


Fig. 1: Schematic edge-on view of the CMZ modelled as a cylinder of radius $R_{\text{CMZ}} = 200$ pc and height $H_{\text{CMZ}} = 100$ pc, centred around Sgr A*. The average density inside the CMZ is $n_{\text{CMZ}} = 1.5 \times 10^2 \text{ cm}^{-3}$. The densities in the Galactic disc and halo are taken as $n_{\text{disk}} \sim 1 \text{ cm}^{-3}$ and $n_{\text{out}} \sim 10^{-2} \text{ cm}^{-3}$.

The CMZ has been detected in very high-energy γ -rays (Aharonian et al. 2006). The spatial correlation between the observed γ -rays and the gas distribution in the region suggests that such emission is due to the decay of neutral pions produced in inelastic interactions between CRs and ambient gas. Moreover, a study of the morphology of the γ -ray emission suggests that the CRs responsible for such emission have been produced in the past by an accelerator located very close to the GC and that such an accelerator continuously injects relativistic particles into the surrounding medium (HESS Collaboration et al. 2016).

After the escape from the accelerator, the transport of relativistic particles in and around the CMZ is dictated by spatial diffusion in the turbulent ambient magnetic field and advection in the Galactic wind. At the same time, particles suffer energy losses due to interactions with ambient matter and radiation and are re-accelerated due to scattering off ambient magnetohydrodynamic waves.

In order to describe the transport of CRs in the CMZ region, it is convenient to adopt a cylindrical set of co-ordinates centred on the GC, with the radial co-ordinate, r , directed along

Table 1: Physical parameters adopted to model the CMZ.

Parameter	Value
D_{GC}	8.5 kpc
R_{CMZ}	2.0×10^2 pc
H_{CMZ}	1.0×10^2 pc
V_{CMZ}	$3.4 \times 10^{62} \text{ cm}^3$
M_{CMZ}	$6 \times 10^7 M_{\odot}$
n_{CMZ}	$1.5 \times 10^2 \text{ cm}^{-3}$
n_{disk}	1.0 cm^{-3}
n_{out}	$1.0 \times 10^{-2} \text{ cm}^{-3}$
$D(10 \text{ TeV})$	$6 \times 10^{29} \text{ cm}^2 \text{ s}^{-1}$
β	0.3
B_{CMZ}	$1.5 \times 10^2 \mu\text{G}$
B_{disk}	$3.0 \mu\text{G}$
B_{out}	$3.0 \mu\text{G}$
v_{A}	$1.0 \times 10^2 \text{ km s}^{-1}$
v_{w}	$2.0 \times 10^2 \text{ km s}^{-1}$
$T_{\text{NIR}} (\kappa_{\text{NIR}})$	0.3 eV (1.3×10^{-11})
$T_{\text{FIR}} (\kappa_{\text{FIR}})$	6×10^{-3} eV (9×10^{-6})
$T_{\text{CMB}} (\kappa_{\text{CMB}})$	2.35×10^{-4} eV (0.99)

the Galactic plane and the height, z , orthogonal to it. The equation describing the evolution in time, space, and momentum of the CR particle distribution function, $f(t, r, z, p)$, is (Berezinskii et al. 1990):

$$\begin{aligned} \frac{\partial f}{\partial t} = & D_{rr} \frac{\partial^2 f}{\partial r^2} + \left(\frac{D_{rr}}{r} + \frac{\partial D_{rr}}{\partial r} \right) \frac{\partial f}{\partial r} + D_{zz} \frac{\partial^2 f}{\partial z^2} + \frac{\partial D_{zz}}{\partial z} \frac{\partial f}{\partial z} - v_{\text{w}} \frac{\partial f}{\partial z} \\ & + \frac{1}{p^2} \frac{\partial}{\partial p} \left(p^2 D_{pp} \frac{\partial f}{\partial p} \right) + \frac{p}{3} \frac{\partial v_{\text{w}}}{\partial z} \frac{\partial f}{\partial p} - \frac{1}{p^2} \frac{\partial}{\partial p} (\dot{p} p^2 f) + Q \end{aligned} \quad (8)$$

where D_{rr} and D_{zz} are the CR spatial diffusion coefficients along r and z , respectively, v_{w} is the Galactic wind velocity (assumed to be directed along the z axis), D_{pp} the CR diffusion coefficient in momentum (particle re-acceleration), \dot{p} the momentum loss rate, and Q the particle injection rate. In the following, we consider the case of an isotropic and spatially uniform diffusion ($D(p) = D_{rr} = D_{zz}$) and a wind speed that is independent of z .

The first four terms on the right-hand side of Eq.8 describe the spatial diffusion of particles, while the fifth term refers to advection in the Galactic wind. Diffusion in momentum space (re-acceleration) is modelled by the sixth term, while the seventh represents adiabatic losses. Finally, the eighth term accounts for momentum losses at a rate, \dot{p} , due to particle interaction with ambient matter and radiation.

The CR spatial diffusion coefficient is difficult to constrain from observations. However, in order to have diffusive transport of CRs in the CMZ, the mean free path for spatial diffusion has to be much smaller than the size of the region, R_{CMZ} . This converts into an upper limit for the CR diffusion coefficient as $D \ll cR/3 \approx 6 \times 10^{30} \text{ cm}^2 \text{ s}^{-1}$. Following HESS Collaboration et al. (2016), we assume the diffusion to be isotropic, and the diffusion coefficient is

$$D_{rr} = D_{zz} = D(p) = 6 \times 10^{29} \left(\frac{pc}{10 \text{ TeV}} \right)^{\beta} \text{ cm}^2 \text{ s}^{-1}, \quad (9)$$

with $\beta = 0.3$. Although theoretical considerations suggest that a break might appear in $D(p)$ in the low-energy (transrelativistic) regime (see e.g. Phan et al. 2021, and references therein),

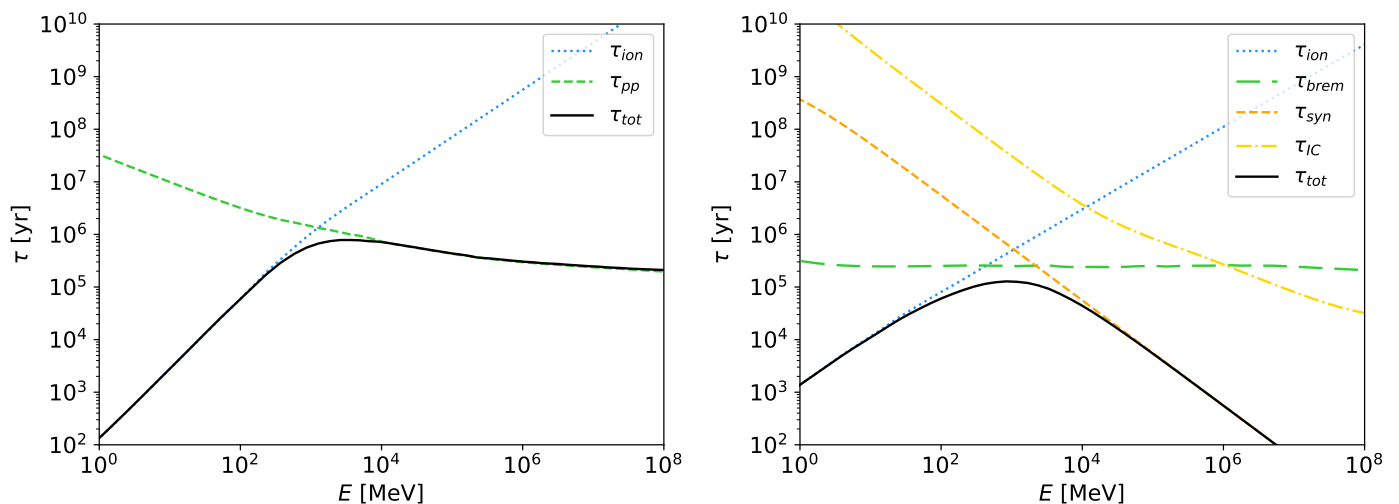


Fig. 2: Characteristic timescales for CR energy losses in the CMZ (see Tab. 1 to see what parameters were adopted). Proton loss times for ionisation and p-p interactions (left panel) and electron loss times for ionisation, synchrotron, bremsstrahlung, and inverse Compton scattering (right panel).

we adopt here a pure power law scaling down to arbitrarily low particle energies, as the presence of a break will not affect any of our results. Our choice of D makes the transport of CRs diffusive up to particle energies in the multi-peta-electronvolt domain.

The advection of CRs is caused by a Galactic wind with a discontinuous velocity at $z = 0$ of the form $v(z) = \text{sgn}(z)v_w$. The value of the wind speed, v_w , in the CMZ region is uncertain, with estimates ranging from 200 km s^{-1} to 1200 km s^{-1} (see e.g. Crocker et al. 2011). To maximise the impact of CRs in the region, we adopt here the value corresponding to the lower bound in that interval: $v_w \sim 200 \text{ km s}^{-1}$. Larger values of v_w would increase advection efficiency, resulting in lower densities of CRs in the CMZ region.

The CR momentum diffusion coefficient, D_{pp} , is expected to be inversely proportional to the spatial diffusion coefficient, as many repeated scatterings onto (moving) magnetic irregularities would enhance diffusion in momentum space while suppressing spatial diffusion. If magnetic perturbances are Alfvén waves, the following heuristic expression can be adopted (Thornbury & Drury 2014):

$$D_{pp}(p) = \frac{p^2 v_A^2}{9D(p)}, \quad (10)$$

where v_A is the Alfvén velocity.

The momentum loss rate, \dot{p} , accounts for energy loss processes due to interactions of CRs with ambient matter and radiation (see Padovani et al. 2018; Gabici 2022, and references therein). It describes ionisation losses at low particle energies, while at larger energies, bremsstrahlung, synchrotron, and inverse Compton losses dominate for CR electrons and proton-proton inelastic interactions for CR protons.

Ionisation, pion production, and bremsstrahlung losses depend only on the ambient gas density and are treated in the following as in Padovani et al. (2018). To describe inverse Compton losses, we followed Khangulyan et al. (2014) and considered a target photon field with three thermal (grey body) components: near-infrared (NIR), far-infrared (FIR), and the cosmic microwave background (CMB), equal to the ones adopted by Hinton & Aharonian (2007) to model the radiation density in the CMZ region. For synchrotron losses, the value of the ambient

magnetic field, B , was kept as a free parameter, but its value was constrained to be larger than $50 \mu\text{G}$, a lower limit derived observationally for the CMZ by Crocker et al. (2010). The magnetic field strength outside the CMZ was taken to be $5 \mu\text{G}$. Although higher values have been suggested by Orlando & Strong (2013); Planck Collaboration et al. (2016); Orlando (2019), the choice of this value does not affect our results. The energy loss time for each mechanism, l , was then defined as

$$\tau_l = E/\dot{E}, \quad (11)$$

where E is the particle kinetic energy and $\dot{E} = -dE/dt$ the energy loss rate. The loss times are shown in Fig. 2 for CR protons (left) and electrons (right).

Finally, the injection of CR particles was considered to be point-like in space and continuous in time. Particle spectra were assumed to be power laws (or broken power laws, as in Sec. 4) in momentum, giving:

$$Q_i(r, z, p) = Q_{p,i}(p) \frac{\delta(r)}{2\pi r} \delta(z), \quad (12)$$

where

$$Q_{p,i}(p) = Q_{0,i} \left(\frac{pc}{10 \text{ TeV}} \right)^{-\delta_i}, \quad (13)$$

where the subscript i can refer to either protons ($i = p$) or electrons ($i = e$).

For each process affecting the propagation of CRs, it is possible to define a characteristic timescale based on the geometry of the CMZ and the typical physical parameters that characterise that region (see Tab. 1). This gives us an idea of the relative importance of a mechanism at any given energy (see Fig. 3, where all relevant timescales are shown).

The timescale for spatial diffusion was defined as the time needed for a CR of momentum p to diffuse across a distance of R_{CMZ} :

$$\tau_{\text{diff}}(p) = \frac{R_{\text{CMZ}}^2}{6D(p)}. \quad (14)$$

The advection timescale was defined as the time needed for a particle to be advected over a vertical distance of $H_{\text{CMZ}}/2$:

$$\tau_{\text{adv}}(p) = \frac{H_{\text{CMZ}}}{2v_w}. \quad (15)$$

The timescale for re-acceleration was defined as the time required for a particle to reach a momentum, p :

$$\tau_{\text{reac}}(p) = \frac{p^2}{6D_{pp}(p)}. \quad (16)$$

The ratio between the re-acceleration and diffusion timescale is

$$\frac{\tau_{\text{reac}}}{\tau_{\text{diff}}} = \frac{9D^2}{v_A^2 R_{\text{CMZ}}^2} \sim 1.6 \times 10^3 \left(\frac{D}{10^{28} \text{ cm}^2/\text{s}} \right)^2 \left(\frac{v_A}{10 \text{ km/s}} \right)^{-2}, \quad (17)$$

which is large for any plausible value of the Alfvén speed and of the diffusion coefficient. Indeed, re-acceleration is not a relevant process at any energy scale of our interest (see Fig. 3). Therefore, in the following, we have fixed $v_A = 100 \text{ km s}^{-1}$ both inside and outside the CMZ as this parameter does not significantly affect our results. It has been verified that adopting $v_A = 0 \text{ km s}^{-1}$ does not give any observable differences in the CR spectra. Finally, the loss timescale was calculated separately for protons and electrons using the loss times (Eq. 11) for all the mechanisms considered.

The steady-state solution for a given injection spectrum was obtained by solving the transport equation numerically with a Crank-Nicholson scheme (Evoli et al. 2017; Kissmann 2014; Press et al. 1992) in which the delta-function in space describing particle injection (Eq. 12) was modelled as a narrow Gaussian. The physical parameters adopted to compute all the characteristic times are given in Table. 1.

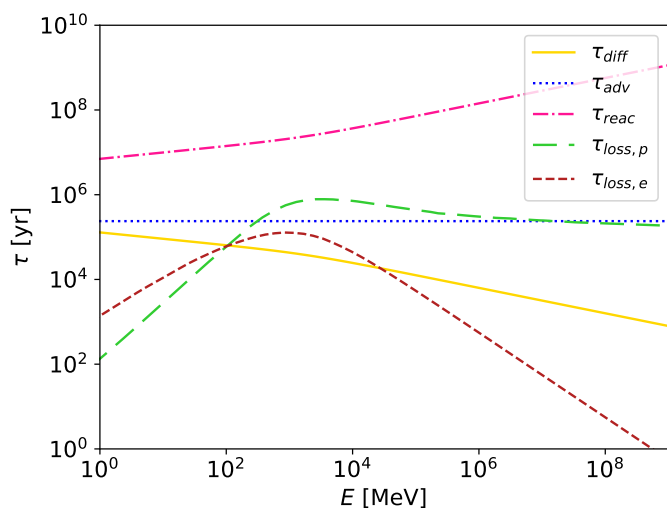


Fig. 3: Characteristic timescales for spatial diffusion, advection, re-acceleration, and losses for protons and electrons. The fiducial parameters are given in Table. 1.

3. γ -ray observations of the central molecular zone

The γ -ray emission from the CMZ has been observed by the High Energy Stereoscopic System (H.E.S.S.) (Aharonian et al. 2006; HESS Collaboration et al. 2016; H. E. S. S. Collaboration et al. 2018), the Fermi Gamma-ray Space Telescope (Gaggero

et al. 2017), the Very Energetic Radiation Imaging Telescope Array System (VERITAS) (Adams et al. 2021), and the Major Atmospheric Gamma Imaging Cherenkov (MAGIC) Telescopes (MAGIC Collaboration et al. 2020). In the following, we compare our predictions with the observations performed by Fermi in the region of Galactic co-ordinates $|l| < 0.8^\circ$ and $|b| < 0.3^\circ$ (Gaggero et al. 2017) and by H.E.S.S. in the regions defined by $|l| < 0.8^\circ$ and $|b| < 0.3^\circ$ (Aharonian et al. 2006) and $|l| < 1^\circ$ and $|b| < 0.3^\circ$ (H. E. S. S. Collaboration et al. 2018).

The γ -rays observed from the Galactic disc result from the interactions of CRs with matter and radiation in the interstellar medium. The dominant process of γ -ray production is the interaction of CR protons with nuclei in the ISM. Leptonic processes such as inverse Compton scattering and non-thermal bremsstrahlung might also contribute to the γ -ray emission (though they are expected to be subdominant in the CMZ).

The CMZ region is characterised by a very large gas density, and its γ -ray emission correlates quite well with the spatial distribution of interstellar matter, pointing quite unambiguously to a hadronic origin of the observed γ -rays (Aharonian et al. 2006). A more detailed analysis of the H.E.S.S. data suggests that the γ -ray emission is produced by CR nuclei that escaped from an accelerator located very close to the GC, which has been injecting particles in the surrounding medium for an extended period of time.

In the remainder of this section, we make use of the CR transport code described in Sec. 2 and we estimate the γ -ray emission produced by CR nuclei and electrons that have been produced by such a source and that are now filling the CMZ.

In order to estimate the spectrum of γ -rays produced in hadronic proton-proton interactions, we make use of the parameterisations of cross-sections provided by Kafexhiu et al. (2014), including the nuclear enhancement factor that accounts for the presence of nuclei heavier than protons in both CRs and interstellar matter.

To model inverse Compton scattering, we considered interactions between relativistic electrons and soft photons present in the CMZ, following the approach presented in Khangulyan et al. (2014). The thermal components of the radiation field in the CMZ are NIR, peaking at a photon energy of 0.3 eV, FIR at 6×10^{-3} eV, and the CMB at 2.35×10^{-4} eV (Hinton & Aharonian 2007). The respective energy densities are 9, 1, and 0.26 eV cm^{-3} . Each component was assumed to be characterised by a diluted black-body spectrum, with the dilution factor, κ , computed using the Stefan-Boltzmann law:

$$\kappa = \frac{wC}{4\sigma_{\text{sb}}T^4}, \quad (18)$$

where w is the photon energy density, c the speed of light, σ_{sb} the Stefan-Boltzmann constant, and T the photon temperature.

Finally, bremsstrahlung radiation is produced when electrons decelerate in the Coulomb field of an ion. The emitted γ -ray radiation was modelled using the cross-section appropriate for interactions of energetic electrons with neutral molecular hydrogen given in Schlickeiser (2002).

Derivation of cosmic-ray proton injection spectrum

In this section, we make use of the CR transport code described above to model the propagation of CRs that escaped the accelerator located in the GC and now fill the CMZ region. The time-dependent Eq. 8 was evolved in time until stationarity was reached. Then, the γ -ray emission from interactions of both CR

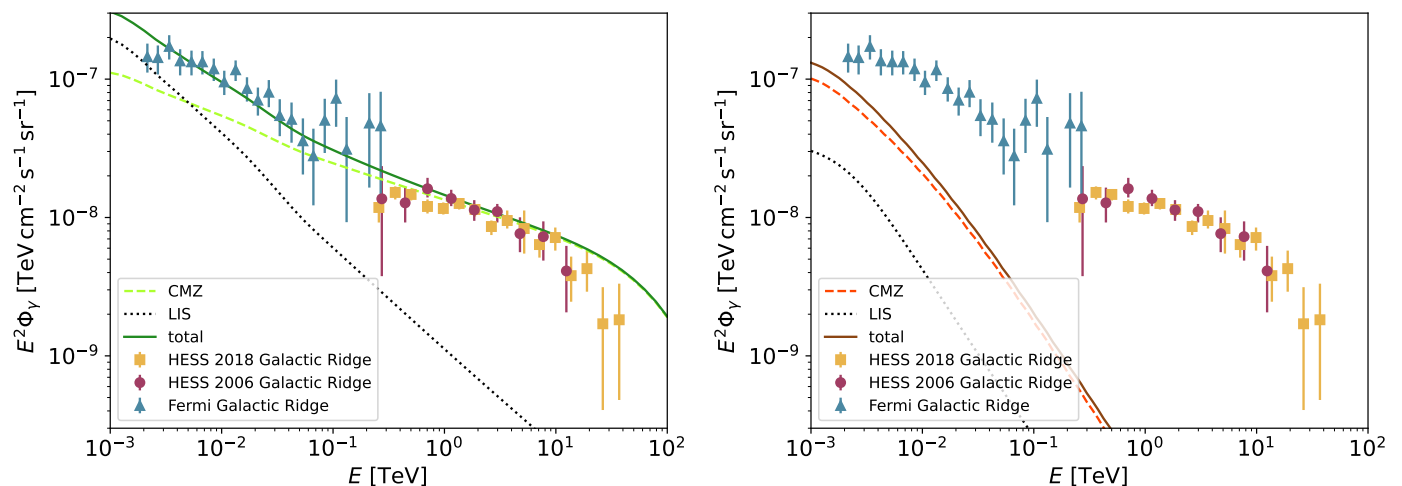


Fig. 4: γ -ray data for the CMZ region. Curves show theoretical results for hadronic (left panel) and leptonic (right panel) scenarios. Dashed lines show the emission from CRs accelerated within the CMZ (in a source located at the GC), while dotted lines show the contribution from ambient CRs, assumed to have a spectrum equal to the local interstellar one (LIS).

nuclei and electrons in the ISM was computed. The spatial correlation between the γ -ray emission and the distribution of dense gas in the CMZ suggests a hadronic origin of the γ -ray photons (HESS Collaboration et al. 2016). So, the fit to available data allows us to derive the injection spectrum for CR protons. We also consider and critically discuss leptonic scenarios in which the γ -ray data is used as an upper limit for the contribution from inverse Compton scattering and relativistic bremsstrahlung.

The left and right panels of Fig. 4 show the observed γ -ray spectrum of the CMZ region, together with curves showing the results of our hadronic and leptonic models obtained by solving Eq. 8. Data points refer to Fermi and H.E.S.S. observations, as is indicated in the figure inset. As we show in the same plot γ -ray brightnesses extracted from slightly different regions, we decided to compare them with a typical predicted brightness computed for the entire CMZ (model curves in the figure). Such an approach, admittedly approximate, introduces uncertainty in our derived CR spectrum normalisation of the order of a few tens of percent. This is not a concern, given that we are seeking to explain an excess of several orders of magnitude in the CR ionisation rate. We note that the same caveat applies to the fit to radio data presented in Fig. 5.

The model curves shown in the figure refer to the emission from CR nuclei (left panel) and CR electrons (right panel). The long dashed lines show our predictions for the γ -ray emission generated by CRs accelerated by the source located in the GC. Dotted lines show the emission coming from the interactions of background Galactic CRs that are known to fill the entire Galactic disc. As the spatial gradient of the latter component is believed to be very small, we assume that background CRs have the same intensity as the ones measured in the local interstellar medium (the label LIS stands for local interstellar spectrum) by Voyager and AMS-02 (see e.g. Gabici 2022, and references therein):

$$J_{\text{LIS,p}}(E_p) = \frac{J_{0,p} \left(\frac{E_p}{\text{MeV}} \right)^{0.35}}{\left[1 + \left(\frac{E}{80 \text{ MeV}} \right)^{1.3} \right] \left[1 + \left(\frac{E_p}{2.2 \text{ GeV}} \right)^{1.9/s} \right]^s}, \quad (19)$$

where $J_{0,p} = 12.5 \text{ MeV}^{-1} \text{ m}^{-2} \text{ s}^{-1} \text{ sr}^{-1}$ and $s = 2.1$.

The γ -ray emission from background CR nuclei dominates the flux in the giga-electronvolt energy domain, but it becomes subdominant in the tera-electronvolt one. On the other hand, the emission from background CR electrons is always largely subdominant.

From Fig. 4 (left panel), it can be seen that the hadronic scenario provides a good fit to γ -ray data if the injection spectrum of CR protons is characterised by:

$$Q_{p,p}(10 \text{ TeV}) = 1.1 \times 10^{29} \text{ MeV}^{-1} \text{ s}^{-1} \quad (20)$$

$$\delta_p = 4.1. \quad (21)$$

This corresponds to a CR proton luminosity above particle energy of 10 TeV equal to $W_{\text{CR}}(E_p \geq 10 \text{ TeV}) \approx 7 \times 10^{37} \text{ erg s}^{-1}$, which is comparable with the early estimation from the H.E.S.S. Collaboration $\approx 4 \times 10^{37} (D(10 \text{ TeV})/10^{30} \text{ cm}^2 \text{ s}^{-1}) \text{ erg s}^{-1}$ (HESS Collaboration et al. 2016). The leptonic scenario (right panel of Fig. 4) will be discussed in the next section.

4. Radio observations of the central molecular zone

The radio emission from the CMZ region has been mapped by the Very Large Array (VLA) (LaRosa et al. 2005), the Green Bank Telescope (GBT) (Law et al. 2008), and MeerKAT (Heywood et al. 2022). We consider here the total continuum flux at 0.325, 1.40, 8.5, and 5 GHz obtained by Law et al. (2008), Yusef-Zadeh et al. (2013) from the inner $2^\circ \times 0.85^\circ$ of the GC region. According to Law et al. (2008) and Yusef-Zadeh et al. (2013), the contribution from non-thermal emissions at these frequencies – that is, synchrotron radiation from CR electrons – is largely dominant. Hence, the radio continuum emission can be used to probe the intensity of CR electrons close to the GC.

Derivation of the cosmic-ray electron spectrum

Here, we constrain the spectrum of CR electrons in the CMZ from the radio observations of the inner from the GBT (Law et al. 2008; Yusef-Zadeh et al. 2013). To fit this data, we assumed that CR electrons are injected at the central source with a spectrum

that is a broken power law in momentum:

$$Q_{p,e}(p) = \begin{cases} Q_* \left(\frac{p}{p_*}\right)^{-\delta_{e,1}}, & \text{if } p \leq p_* \\ Q_* \left(\frac{p}{p_*}\right)^{-\delta_{e,2}}, & \text{otherwise} \end{cases}, \quad (22)$$

where $p_*c = 1.5$ GeV. Similarly to the case of γ -ray emissions, we propagated this injection spectrum using Eq.(8) and the steady-state solution was used to compute synchrotron emissions.

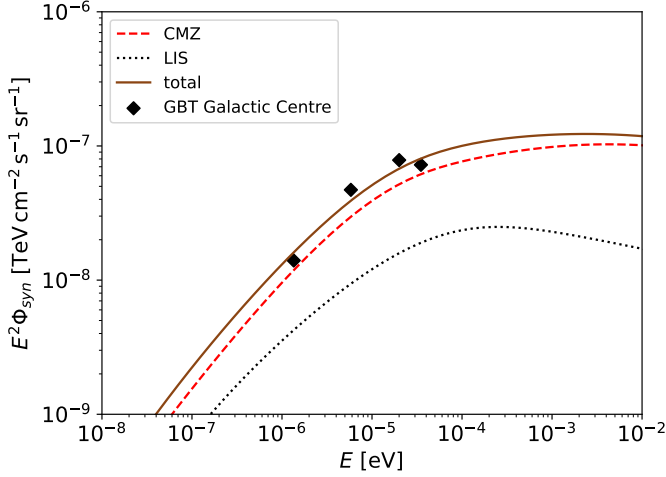


Fig. 5: Fit to radio data from the CMZ region. The solid line refers to the total predicted synchrotron emission from CR electrons. The dashed line shows the contribution from electrons accelerated inside the CMZ. The dotted line shows the contribution from the background sea of CR electrons (LIS) with a low-energy exponential cut-off to take into account the suppressed penetration of background CR electrons into the CMZ. We consider an average magnetic field strength of $B_{\text{CMZ}} \sim 150 \mu\text{G}$.

The radio data can be fitted using a broken power law, as is defined in Eq.(22) using the following normalisation:

$$Q_{p,e}(10 \text{ TeV}) = 1.5 \times 10^{27} \text{ MeV}^{-1} \text{ s}^{-1}, \quad (23)$$

and spectral indices

$$\delta_{e,1} = 3.25 \quad (24)$$

$$\delta_{e,2} = 4.4, \quad (25)$$

where $\delta_{e,1}$ is mostly constrained by radio data, while $\delta_{e,2}$ has been chosen to not overshoot the γ -rays. In this respect, the right panel of Fig.(4) shows the observed γ -ray spectrum of the CMZ plotted with the contributions expected from inverse Compton and relativistic bremsstrahlung produced by the steady-state spectrum obtained from Eq.(22).

To the contribution from the CRs accelerated in the GC, we added the radio emission from the background Galactic CR electrons. The intensity of the background CR electrons, obtained from Voyager and AMS-02 data (see e.g. Gabici 2022, and references therein), is:

$$J_{\text{LIS},e}(E_e) = \frac{J_{0,e} \left(\frac{E}{\text{MeV}}\right)^{-1.3} \exp\left(-\frac{100 \text{ MeV}}{E_e}\right)}{\left[1 + \left(\frac{E}{65 \text{ MeV}}\right)^{0.6/s_1}\right]^{s_1} \left[1 + \left(\frac{E}{2.8 \text{ GeV}}\right)^{1.38/s_2}\right]^{s_2}}, \quad (26)$$

where $J_{0,e} = 5 \times 10^3 \text{ MeV}^{-1} \text{ m}^{-2} \text{ s}^{-1} \text{ sr}^{-1}$, $s_1 = 0.2$ and $s_2 = 0.5$.

Before computing the synchrotron emission from the ambient (LIS) CRs, we added a low-energy exponential cut-off at an energy of 100 MeV. This is the energy for which the CR electron loss time equals the diffusion time across the CMZ (see Fig. 3), and the cut-off is intended to roughly mimic the effect of the penetration of Galactic CRs into the CMZ (see e.g. Dogiel et al. (2021)).

5. Cosmic-ray ionisation rate

Once we had imposed constraints on the intensity and spectral energy distribution of CR nuclei and electrons in the CMZ, we investigated the impact that these particles have on the gas in the CMZ. In particular, we computed the CR ionisation rate of ambient gas, and we compared that with available measurements of this parameter. To do so, it was necessary to extrapolate to low energies the CR spectra derived above, as low-energy particles (roughly in the sub-giga-electronvolt domain) are believed to be the most effective ionisation agents in MCs.

As is described in Sec. 1, the ionisation rate of H_2 molecules in dense MCs can be measured by means of observation of molecular lines such as, most notably, those of H_3^+ falling in the IR band (Oka 2006; Miller et al. 2020). This is because the production of H_3^+ in MCs follows in a straightforward way from the ionisation of molecular hydrogen.

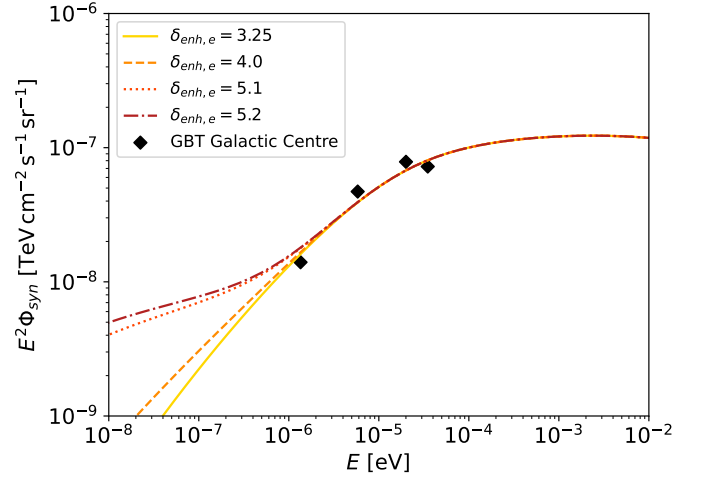


Fig. 6: Expected synchrotron radio emission from the enhanced CR electron injection spectra considered in this work (see main text for details), compared to radio observations of the CMZ.

If f_p and f_e are the CR particle distribution functions for protons and electrons, respectively, the CR proton and electron ionisation rates can be expressed as:

$$\begin{aligned} \zeta_p &= \int_{E_{\min}}^{E_{\max}} v_p f_p(E_p) \sigma_p^{\text{ion}}(E_p) (1 + \phi_p(E_p)) dE_p \\ &+ \int_0^{E_{\max}} v_p f_p(E_p) \sigma_p^{e.c.}(E_p) dE_p \\ \zeta_e &= \int_{E_{\min}}^{E_{\max}} v_e f_e(E_e) \sigma_e^{\text{ion}}(E_e) (1 + \phi_e(E_e)) dE_e, \end{aligned} \quad (27)$$

where v_i is the particle velocity, and ϕ_i the average number of secondary ionisations per primary ionisation, modelled as in Krause et al. (2015). Available parameterisations of the proton

impact ionisation cross-section, σ_p^{ion} , the electron capture cross-section, $\sigma_p^{e.c.}$, and the electron impact ionisation cross-sections, σ_e^{ion} , have been reviewed by Padovani et al. (2009) and later improved by Krause et al. (2015) and Gabici (2022). The impact of CR nuclei heavier than protons should also be accounted for when computing the CR ionisation rate. This was done by introducing an enhancement factor, $\eta \approx 1.5$, to make the CR ionisation rate of nuclei (including protons) $\zeta_n = \eta \zeta_p$ (Padovani et al. 2009). In the following, the term proton ionisation rate will refer to the nuclear-enhanced value.

The electron ionisation cross-section peaks in the sub-kilo-electronvolt energy range, and any electron of energy larger than the ionisation potential of H_2 , $I = 15.426$ eV will contribute to ionising the ambient gas. Hence, we considered CR electrons of energy larger than $E_{min} = I$.

On the other hand, for ionisation due to CR protons, electron capture dominates over proton impact for particle energies below a few tens of kilo-electronvolts (see e.g. Fig. 11 in Gabici 2022). This means that a CR proton cooling below that energy will convert into a fast neutral hydrogen atom and, as a consequence, will become unable to further ionise the gas (e.g. Chabot 2016). For this reason, for protons, we set $E_{min} = 45$ keV.

As a first step, the CR proton and electron injection spectra inferred from γ -ray and radio data in the previous section have been extrapolated down to lower energies and propagated using the transport equation solver to obtain steady-state spectra. Then, the CR proton and electron ionisation rates averaged over the entire CMZ volume were computed to find $1.9 \times 10^{-17} \text{ s}^{-1}$ and $3.0 \times 10^{-18} \text{ s}^{-1}$, respectively. These values are much (orders of magnitude) smaller than the measured ones, meaning that an extra component of CRs must be present in order to explain the observations.

The extra component (enhancement) was added to the CR injection spectra derived above in the following way:

$$Q_{p,p}(p) = \begin{cases} Q_{enh,p} \left(\frac{p}{p_{enh,p}} \right)^{-\delta_{enh,p}}, & \text{if } p \leq p_{enh,p} \\ Q_{enh,p} \left(\frac{p}{p_{enh,p}} \right)^{-\delta_p}, & \text{otherwise} \end{cases} \quad (28)$$

for protons and

$$Q_{p,e}(p) = \begin{cases} Q_{enh,e} \left(\frac{p}{p_{enh,e}} \right)^{-\delta_{enh,e}}, & \text{if } p \leq p_{enh,e} \\ Q_{enh,e} \left(\frac{p}{p_{enh,e}} \right)^{-\delta_{e,1}}, & \text{if } p_{enh,e} \leq p \leq p_* \\ Q_{enh,e} \left(\frac{p_*}{p_{enh,e}} \right)^{\delta_{e,2} - \delta_{e,1}} \left(\frac{p}{p_{enh,e}} \right)^{-\delta_{e,2}}, & \text{otherwise} \end{cases} \quad (29)$$

for electrons.

For particle momenta below $p_{enh,i}$, CR spectra were enhanced with respect to those adopted so far in this paper. For protons, we chose $p_{enh,p} \approx 780$ MeV. This momentum corresponds to a kinetic energy of $E_p = 280$ MeV, which is the threshold for pion production. Adding an enhancement below this momentum will ensure that no γ -rays are produced by the additional component, and therefore the fits to γ -ray data performed above will be unaffected. For electrons, the transition momentum was chosen to be equal to $p_{enh,e} \approx 450$ MeV, which ensures that the fit to radio data obtained above is unaffected. This can be seen in

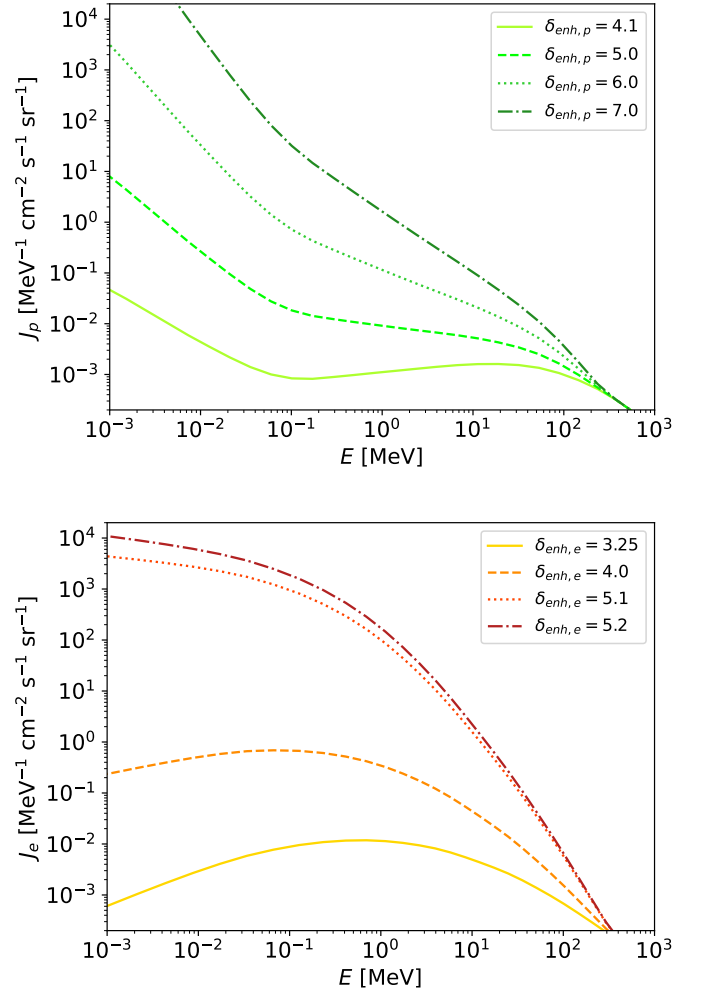


Fig. 7: Steady-state CR intensities for protons (top) and electrons (bottom) averaged over the CMZ volume. Curves refer to different enhancements applied to the CR injection spectrum, as is indicated by the parameter $\delta_{enh,i}$.

Fig. 6, in which the synchrotron radio emission from enhanced electron spectra is shown together with radio data.

The steady-state CR proton and electron intensities averaged over the entire CMZ volume are shown in Fig. 7 for various values of the parameter $\delta_{enh,i}$.

The proton and electron ionisation rates computed using these volume-averaged spectra are shown in Fig. 8 as a function of different minimum ionising particle energies, E_{min} (this is the minimum energy that appears in Eq. 27). For comparison, we have also plotted as a horizontal thick black line the ionisation rate, $\zeta_{H_3^+}$, in the GC region obtained from H_3^+ observations, obtained by averaging the measurements from Le Petit et al. (2016); Oka et al. (2019). We have also added a grey-shaded region, which gives the range of values for the more conservative ionisation rates, ζ_{chem} , inferred from measurements of the abundances of other chemical species (Rivilla et al. 2022; Sanz-Novio et al. 2024).

We see from Fig. 8 that in order to reproduce the ionisation rate measurements, one needs an extremely steep additional CR component (slopes larger than $\delta_{enh,p} \sim 7$ and $\delta_{enh,e} \sim 5$ for CR protons and electrons, respectively) extending down to very low particle energies ($E_{min} \approx 1$ keV – 1 MeV for both CR protons

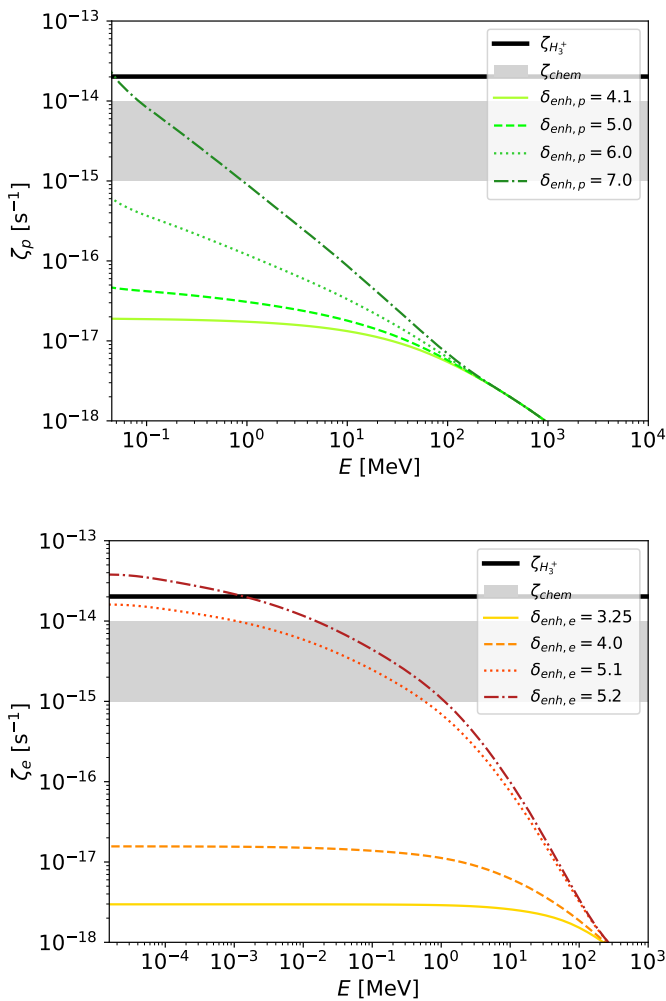


Fig. 8: CR proton (top) and electron (bottom) ionisation rates as a function of the minimum particle energy considered for the CR spectra shown in Fig. 7. Values were averaged over the CMZ volume and compared to the estimated values of ionisation rates derived by different observational methods (horizontal black line and shaded region).

and electrons). Very steep spectra are needed because the energy loss time of CR particles is very short at sub-giga-electronvolt energies (see Fig. 3), and therefore this has to be compensated for by the injection of a very large number of low-energy particles (for a discussion of this issue see Recchia et al. 2019). This raises the question of what energy budget is required to maintain a population of particles capable of reproducing the measured ionisation rate in the CMZ.

To answer this question, we computed two quantities: the power, W_{CR} , needed to maintain the CR population at a given level in the CMZ and the CR energy density averaged over the entire CMZ volume, n_{CR} . These quantities were computed for CR spectra able to reproduce the measurements of the ionisation rates in the CMZ and are reported in Tabs. 2 and 3 for CR protons and electrons, respectively. Here, we note E_{min} , the minimum ionising energy needed for the computed ionisation rate to exceed the measured values.

The powers obtained in this way can be compared with the total CR power of the Milky Way, which can be estimated using the large amount of available CR data. This has been done,

Table 2: Power requirements and energy density for proton spectra as a function of the corresponding proton CR ionisation rate in the CMZ

$\zeta_p (\text{s}^{-1})$	$\delta_{\text{enh},p}$	$E_{\text{min}} (\text{MeV})$	$W_{\text{CR}} (\text{erg s}^{-1})$	$n_{\text{CR}} (\text{eV cm}^{-3})$
10^{-15}	7.0	0.9	$3.7 \cdot 10^{39}$	0.48
$2 \cdot 10^{-14}$	7.0	$4.5 \cdot 10^{-2}$	$6.8 \cdot 10^{40}$	0.52

Table 3: Power requirements and energy density for electron spectra as a function of the corresponding electron CR ionisation rate in the CMZ

$\zeta_e (\text{s}^{-1})$	$\delta_{\text{enh},e}$	$E_{\text{min}} (\text{MeV})$	$W_{\text{CR}} (\text{erg s}^{-1})$	$n_{\text{CR}} (\text{eV cm}^{-3})$
10^{-15}	5.1	0.6	$2.0 \cdot 10^{39}$	0.36
10^{-15}	5.2	1.1	$2.1 \cdot 10^{39}$	0.45
$2 \cdot 10^{-14}$	5.2	$1.5 \cdot 10^{-3}$	$2.4 \cdot 10^{40}$	0.58

among many others, by Strong et al. (2010), who found values in the range of $W_{\text{MW}}^p \sim 6.0 - 7.4 \times 10^{40} \text{ erg s}^{-1}$ and $W_{\text{MW}}^e \sim 1.0 - 1.7 \times 10^{39} \text{ erg s}^{-1}$ for CR protons and electrons, respectively. The comparisons with these figures show that the powers reported in Tabs. 2 and 3 are extremely large.

In order to reproduce the values of the ionisation rate measured in the CMZ, CR electrons should be injected by the source located in the GC at a rate that is larger than the total injection rate of CR electrons in the entire Milky Way. For CR protons, the required power has to be comparable to the total CR proton power of the Milky Way in order to reproduce an ionisation rate of the order of 10^{-14} s^{-1} , and a few percent of it to reproduce an ionisation rate of the order of 10^{-15} s^{-1} . Moreover, this huge amount of energy should have as a unique manifestation the enhancement in the gas ionisation rate in the CMZ region.

One can also compare the CR powers obtained above with characteristic powers connected to the SMBH at the centre of the Milky Way. It has been estimated that the mechanical power needed to inflate the giant ($\geq 10 \text{ kpc}$) bubbles discovered by Fermi (Su et al. 2010) and eROSITA (Predehl et al. 2020) is of the order of $P_b \approx 10^{41} \text{ erg s}^{-1}$, and that the injection of energy should last a few tens of millions of years (Sarkar 2024). This is of the same order as the energy required to maintain a population of CR protons capable of ionising the CMZ gas at a rate of $\approx 10^{-14} \text{ s}^{-1}$ and about four times the energy needed in CR electrons to reach the same rate (see last row of both Tab. 2 and 3). It follows that it is quite challenging to explain the large ionisation rates with CRs, while lower values ($\approx 10^{-15} \text{ s}^{-1}$) might still be acceptable.

However, another observable that should be reproduced is the fact that roughly the same ionisation rate has been obtained by analysing H_3^+ lines from several lines of sight across the CMZ (at least up to 100 pc radius, Indriolo et al. 2015). The ionisation rate measured in this way does not show any clear spatial variation and is indeed compatible with a constant value across the CMZ. This trend cannot be reproduced by our model, as is shown in Fig. 10. There, we plot the CR ionisation rate averaged along the lines of sight lying along the Galactic plane at different distances, R , from the GC. The predicted trend for CR protons (top) and electrons (bottom panel) clearly does not explain observations.

We note here that the mass of the CMZ that has been chosen to derive the values reported in Tabs. 2 and 3, though widely used in the literature, is the maximum amongst the various measurements found in the literature (which is $2 - 6 \times 10^7 M_{\odot}$, as

reported in Dahmen et al. 1998). We repeated our entire study for the lower limit of $M_{\text{CMZ}} = 2 \times 10^7 M_{\odot}$ and found that the power needed to sustain ionisation rates at $\approx 10^{-14} \text{ s}^{-1}$ is also in this case of the order of $\gtrsim 10^{40} \text{ erg s}^{-1}$ for protons and $\gtrsim 10^{39} \text{ erg s}^{-1}$ for electrons. This is because a lower mass (and therefore gas density) would require a higher density of high-energy CRs to explain the γ -ray and radio emissions, but at the same time would reduce the effects of ionisation losses. The two effects then compensate.

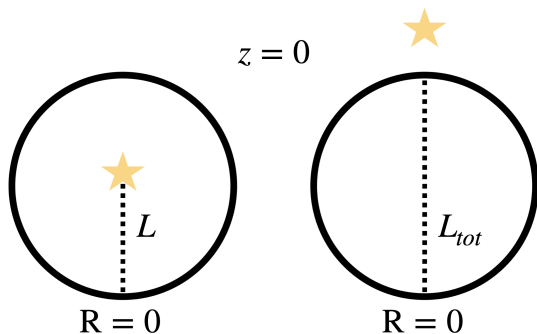


Fig. 9: Position of the star used to measure the column density of H_3^+ with respect to the CMZ. L is the distance from the front of the CMZ to the position of the star. $L_{\text{tot}} = 2R_{\text{CMZ}}$ is the longest distance through the CMZ in any line of sight.

Before concluding, we should notice that the measurements of H_3^+ column densities rely on the presence of a background star. However, the distance to these stars is a major source of uncertainty in the measurements. In fact, the results we presented so far assumed implicitly that the stars are located behind the CMZ (as is illustrated in the right panel of Fig. 9). If, instead, the star is located within the CMZ (as in the left panel of Fig. 9), the average of the predicted CR ionisation rate should be performed over the length, L .

Figure 11 shows the CR ionisation rates averaged from the edge of the CMZ to a depth, L , for lines of sight passing through the point $z = 0$ and $R = 0$. In such a plot, the ionisation rate averaged over the entire line of sight is represented by the right-most value of the curves. The figure shows that if the star is located closer to us than the GC, then one would expect to measure much lower ionisation rates, while only a very slight enhancement of the average ionisation rate is expected for locations of $L \gtrsim R_{\text{CMZ}}$. This makes it even more difficult (if not impossible) to explain the large ionisation rates derived from observations. The plot refers to a line of sight passing through the centre of the CMZ ($R = 0$ and $z = 0$), and therefore corresponds to the maximum possible values of the ionisation rate (as is illustrated by Fig. 10).

6. Additional constraints on mega-electronvolt particles

6.1. Mega-electronvolt γ -rays

The CRs in the mega-electronvolt and sub-mega-electronvolt domains contribute the most to the ionisation rate. Electrons of this energy also emit non-thermal bremsstrahlung photons in the hard-X/soft- γ -ray bands. At such energies, the inner Galaxy has been observed by the SPectrometer on INTEGRAL (SPI) and by the imaging Compton telescope COMPTEL. In particular, Bouchet et al. (2008) presented a list of sources detected

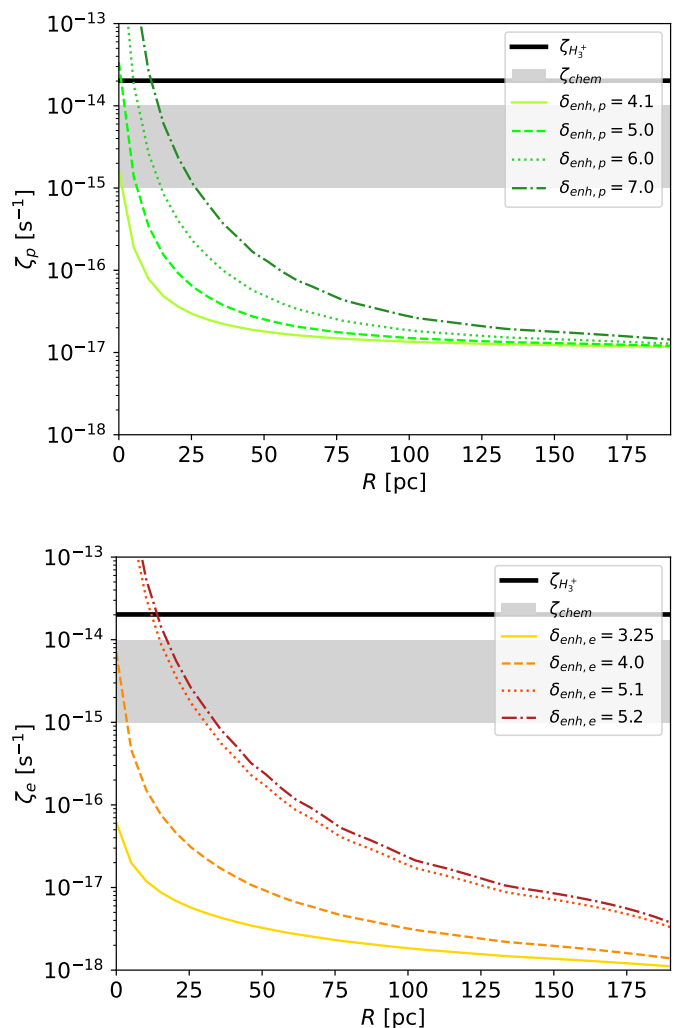


Fig. 10: CR proton (top) and electron (bottom) ionisation rates averaged over lines of sight at different projected distances, R , from the GC. The horizontal lines and shaded regions and the values of $\delta_{\text{enh},i}$ are as in Fig. 8.

by SPI at photon energies in the range spanning from 25 keV to 0.6 MeV. Among those, three are located in the CMZ region: 1E 1740.7–2942 ($l = 359.12^\circ$, $b = -0.1^\circ$), SLX 1744–299 ($l = 359.28^\circ$, $b = -0.9^\circ$), and IGR J17475–2822 ($l = 0.61^\circ$, $b = -0.1^\circ$). The fluxes of these sources in several distinct energy bands can be found in Tab.1 in Bouchet et al. (2008). From that table, we also searched for the weakest detected source in the inner Galaxy, and we took that flux as a proxy for the instrument sensitivity.

We predict a flux for the CMZ (for the case $\delta_e = 5.2$) equal to $4 \times 10^{-2} \text{ keV cm}^{-2} \text{ s}^{-2}$ in the 25 – 50 keV band, $5 \times 10^{-2} \text{ keV cm}^{-2} \text{ s}^{-2}$ in the 50 – 100 keV band, $6 \times 10^{-2} \text{ keV cm}^{-2} \text{ s}^{-2}$ in the 100 – 200 keV band, and $8 \times 10^{-2} \text{ keV cm}^{-2} \text{ s}^{-1}$ in the 200 – 600 keV band. These fluxes are larger than the instrument sensitivity for point sources, and even larger than some of the fluxes of the three sources detected in the CMZ and listed above. In particular, the flux detected by SPI from IGR J17475–2822, associated with the Sgr B2 MCs, is known to decline with time (Terrier et al. 2010). This is not compatible with a CR-related origin of the emission.

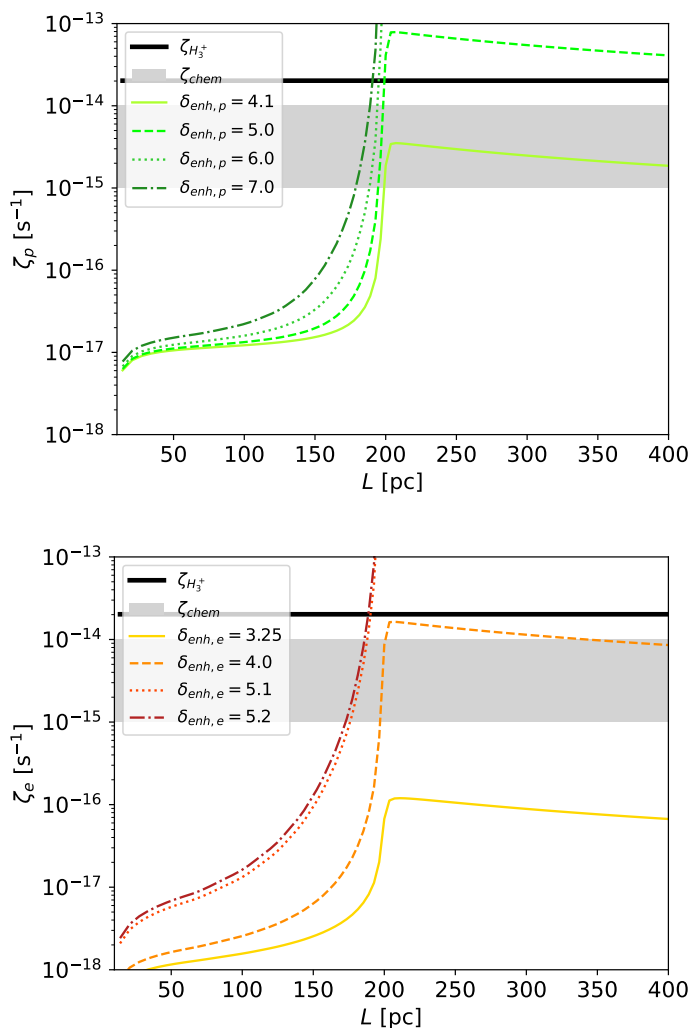


Fig. 11: CR proton (top) and electron (bottom) ionisation rates averaged over different lengths of lines of sight. The horizontal lines and shaded regions and the values of $\delta_{\text{enh},i}$ are as in Fig. 8.

To conclude, if the spectra predicted by our model were the reality, the CMZ would have been detected by SPI as a steady source of mega-electronvolt γ -rays with a centroid around $l = 0^\circ$ and $b = 0^\circ$. Hence, the conclusion stands that mega-electronvolt γ -ray detection does not support the CR ionisation model.

6.2. Iron $K\alpha$ line

The X-ray emission line at 6.4 keV results from the ionisation of iron atoms by the ejection of a K-shell electron. The diffuse X-ray emission from the CMZ has a variable and a constant component. The variable component is believed to be the reflection by the MCs of a past X-ray outburst from the SMBH, which is why it is decreasing over time (Terrier et al. 2018). A constant component is expected from the supposed constant density of CRs ionising the region (Capelli et al. 2012). Since the observations of the CMZ over several years show a decreasing flux, the most recent measurement of the Fe $K\alpha$ line flux is only an upper limit for the contribution from the CRs. The most recent observation of the inner 300 pc was conducted by XMM-Newton in 2012. Other more recent surveys of specific regions exist (Kuznetsova et al. 2022). The XMM-Newton survey has revealed that the

6.4 keV line flux in 2012 was $1.507 \pm 0.009 \times 10^{-3}$ ph cm $^{-2}$ s $^{-1}$ from a 19×112 arcmin 2 area (Terrier et al. 2018). As this region is very similar to the CMZ region, we may compare the average surface brightness from our model with the one measured by XMM-Newton: the corresponding average surface brightness is $7.36 \pm 0.04 \times 10^{-7}$ ph cm $^{-2}$ s $^{-1}$ arcmin $^{-1}$.

The intensity of the Fe $K\alpha$ line resulting from CR interactions can be expressed as:

$$I_i^{K\alpha} = \frac{M_{\text{CMZ}}}{4\pi D_{\text{GC}}^2 m_{\text{avg}}} \int_{E_{\text{min}}}^{E_{\text{max}}} \eta_{Fe} \sigma_i^{K\alpha}(E_i) v_i f_i(E_i) dE_i, \quad (30)$$

where i represents the species of the CR particle, $\sigma_{K\alpha}^i$ is the K-shell ionisation cross-section by CR species i (Tatischeff et al. 2012) considering the solar abundance of iron ($\eta_{Fe} = 3 \times 10^{-5}$), and $m_{\text{avg}} = 1.4m_{\text{H}}$ is the average particle mass.

We computed the Fe $K\alpha$ average surface brightness from the CMZ using the proton and electron spectra that give ionisation rates above 10^{-15} s $^{-1}$. The values are given in Tables 4 and 5. The iron abundance in the CMZ is expected to be higher than that of the solar neighbourhood. Hence, the values of the Fe $K\alpha$ line emissions are a lower limit for what is expected from the CR spectra.

Table 4: Fe $K\alpha$ average surface brightness from CR protons

ζ_p (s $^{-1}$)	$\delta_{\text{enh},p}$	E_{min} (MeV)	$B_p^{K\alpha}$ (ph cm $^{-2}$ s $^{-1}$ arcmin $^{-2}$)
10^{-15}	7.0	0.9	$5.8 \cdot 10^{-10}$
$2 \cdot 10^{-14}$	7.0	$4.5 \cdot 10^{-2}$	$5.8 \cdot 10^{-10}$

Table 5: Fe $K\alpha$ average surface brightness from CR electrons

ζ_e (s $^{-1}$)	$\delta_{\text{enh},e}$	E_{min} (MeV)	$B_e^{K\alpha}$ (ph cm $^{-2}$ s $^{-1}$ arcmin $^{-2}$)
10^{-15}	5.1	0.6	$7.8 \cdot 10^{-9}$
10^{-15}	5.2	1.1	$8.3 \cdot 10^{-9}$
$2 \cdot 10^{-14}$	5.2	$1.5 \cdot 10^{-3}$	$5.1 \cdot 10^{-8}$

The expected Fe $K\alpha$ surface brightness over the CMZ resulting from CR ionisation is lower by a few orders of magnitude than the observed rate. This estimate may increase if the correct iron abundance is used instead of solar abundance, but the enhancement would be, at most, a few factors, and therefore not sufficient to enhance our prediction of the observed values. Hence, Fe $K\alpha$ line observations cannot help to constrain the spectrum of low-energy CRs in the CMZ. Indeed, this agrees with what was claimed by Dogiel et al. (2013), in which it was argued that the contribution to the 6.4 keV line from low-energy CRs responsible for the high ionisation rates must be negligible.

7. Discussion and conclusion

The main conclusion of this paper is that it is extremely unlikely that CRs in the CMZ are the agents responsible for the large ionisation rates derived from a number of observations. Motivated by the results coming from γ -ray observations of the CMZ, we investigated a scenario in which a powerful accelerator of CR is located in the centre of the Galaxy. The accelerator is assumed to continuously inject CRs in the surrounding medium. Once injected, CRs diffuse away from the GC and fill the CMZ.

Fitting the γ -ray and radio emission from the CMZ allowed us to constrain the high-energy spectra of CR particles there.

We found that a simple power-law extrapolation of such spectra at low energies fails by orders of magnitude to reproduce the measured values of the ionisation rate of molecular hydrogen.

We then added an additional, steep, low-energy CR component in an attempt to explain the large values of the ionisation rate without violating any other observational constraint. We showed that the injection power of energetic particles required to explain ionisation rates at the level of $\approx 10^{-14} \text{ s}^{-1}$ is exceedingly large: $\sim 7 \times 10^{40} \text{ erg s}^{-1}$ for protons and $\sim 2 \times 10^{40} \text{ erg s}^{-1}$ for electrons. This is comparable to the total power, P_b , required to inflate the giant eROSITA bubbles. More conservative estimates of the ionisation rate ($\approx 10^{-15} \text{ s}^{-1}$) could be explained if a few percent of the power, P_b , could be somehow converted into CRs.

In fact, this unrealistically large power estimation for low-energy CRs is obtained when using the most conservative values for the transport parameters. We have chosen the diffusion coefficient, the Galactic wind velocity, and the Alfvén speed to maximise the duration for which CRs stay within the CMZ. Hence, we argue that using different values for all these parameters would further increase the power required.

However, the CR energy budget is not the only issue. The CRs escaping from an accelerator located at the GC would generate an ionisation rate that declines quite steeply as the distance from the GC increases. This is not observed in the data, which show a roughly constant value of the ionisation rate throughout the CMZ. Uncertainties in the exact location of the stars used make it even more difficult to fit our model results to the data. In fact, these high ionisation rates are also expected in the cores of dense MCs, and Yang et al. (2023) show that CRs below $\lesssim \text{GeV}$ are prevented from entering such MCs.

We note that the CR energy densities found in our model (see last column of Tabs. 2 and 3) are quite modest. This was also pointed out in a previous study by Dogiel et al. (2015). However, we have stressed here that the power needed to maintain these modest energy densities of CRs is extremely large, mainly due to the very short energy loss time of sub-relativistic particles (see Fig. 2 and times), and that this makes a CR origin of the large ionisation rates very unlikely.

A different scenario could be envisaged whereby an impulsive rather than continuous source of CRs is present. In that case, however, the large ionisation rates would be a transient phenomenon, and this would add an additional parameter (i.e. the time since the impulsive injection) to be fine-tuned. An inspection of Fig. 3 can help in characterising what could be the optimal set-up for this scenario. The duration of the enhanced ionisation rates would be of the order of $\Delta t \lesssim 10^5 \text{ yr}$, which is the characteristic diffusion time of $\approx 100 \text{ MeV}$ CRs across the CMZ. Such particles would lose their energy in a time comparable to the diffusion time across the CMZ. A naive but probably not too inaccurate estimate of the total required energy in this scenario is given by the product $\mathcal{E}_{\text{tot}} \approx W_{\text{CR}} \times \Delta t$, where for W_{CR} one can adopt the values reported in Tab. 3 and 2. This would give $\mathcal{E}_{\text{tot}} \approx 3 \times 10^{52} (W_{\text{CR}}/10^{40} \text{ erg/s})(\Delta t/10^5 \text{ yr}) \text{ erg}$. Remarkably, this is of the same order as the thermal energy of the X-ray chimneys ($\sim 4 \times 10^{52} \text{ erg}$), which are characterised by a sound crossing time equal to $\sim 3 \times 10^5 \text{ yr}$, which is comparable to Δt (Ponti et al. 2019). The chimneys are the exhaust channels through which mass and energy ejected from the SMBH in the GC are channelled out of the Galactic disc. The similarity between their total energy and that needed in low-energy CRs suggests that a scenario based on an impulsive injector of particles would also face severe problems based on global energetic constraints.

Finally, the rough spatial uniformity of the values of the ionisation rate could be explained if many CR sources distributed across the entire CMZ inject energetic particles. In this case, the energy problem could be even more severe, as the source of energy would not be connected to the SMBH located at the GC. As an example, the rate at which mechanical energy is injected in the CMZ due to supernova explosions is $\approx 10^{40} \text{ erg s}^{-1}$ (see Jouvin et al. 2017, and references therein), which is one order of magnitude smaller than P_b .

We conclude that a source of ionisation of molecular hydrogen in the CMZ other than CRs is very likely to exist. The most obvious candidate is a radiation field made of UV and/or X-ray photons. As it is known that X-ray photons emitted by Sgr A* during outbursts do not suffice to explain the observed ionisation rates (Dogiel et al. 2013), the sources of ionising photons will have to be distributed across the entire CMZ. Further studies in this direction are therefore needed.

Acknowledgements. The authors acknowledge helpful advice on the code from Sebastian-Achim Müller, Francesco Conte, Ludwig M. Böss, Enrico Peretti and Alexandre Inventar. We are also thankful for the inspiring discussions on low-energy CRs in the GC region with Andrea Goldwurm, Marianne Lemoine-Goumard, Denis Allard, Rui-zhi Yang, Richard Tuffs, Jim Hinton, Bing Liu, Adam Ginsburg and Thushara Pillai. This study was supported by the LabEx UnivEarthS, ANR-10-LABX-0023 and ANR-18-IDEX-0001. V.H.M.P. acknowledges support from the Initiative Physique des Infinis (IPI), a research training program of the Idex SUPER at Sorbonne Université. S.G. acknowledges support from Agence Nationale de la Recherche (grant ANR-21-CE31-0028).

References

- Adams, C. B., Benbow, W., Brill, A., et al. 2021, *ApJ*, 913, 115
 Aharonian, F., Akhperjanian, A. G., Bazer-Bachi, A. R., et al. 2006, *Nature*, 439, 695
 Berezhinskii, V. S., Bulanov, S. V., Dogiel, V. A., & Ptuskin, V. S. 1990, *Astrophysics of cosmic rays*
 Bouchet, L., Jourdain, E., Roques, J. P., et al. 2008, *ApJ*, 679, 1315
 Capelli, R., Warwick, R. S., Porquet, D., Gillissen, S., & Predehl, P. 2012, *A&A*, 545, A35
 Caselli, P., Walmsley, C. M., Terzieva, R., & Herbst, E. 1998, *ApJ*, 499, 234
 Chabot, M. 2016, *A&A*, 585, A15
 Crocker, R. M., Jones, D. I., Aharonian, F., et al. 2011, *MNRAS*, 413, 763
 Crocker, R. M., Jones, D. I., Melia, F., Ott, J., & Protheroe, R. J. 2010, *Nature*, 463, 65
 Cummings, A. C., Stone, E. C., Heikkilä, B. C., et al. 2016, *ApJ*, 831, 18
 Dahmen, G., Huttemeister, S., Wilson, T. L., & Mauersberger, R. 1998, *A&A*, 331, 959
 Dogiel, V. A., Chernyshov, D. O., Ivlev, A. V., Kiselev, A. M., & Kopyev, A. V. 2021, *ApJ*, 921, 43
 Dogiel, V. A., Chernyshov, D. O., Kiselev, A. M., et al. 2015, *ApJ*, 809, 48
 Dogiel, V. A., Chernyshov, D. O., Tatischeff, V., Cheng, K. S., & Terrier, R. 2013, *ApJ*, 771, L43
 Evoli, C., Gaggero, D., Vittino, A., et al. 2017, *J. Cosmology Astropart. Phys.*, 2017, 015
 Ferrière, K., Gillard, W., & Jean, P. 2007, *A&A*, 467, 611
 Gabici, S. 2022, *A&A Rev.*, 30, 4
 Gaggero, D., Grasso, D., Marinelli, A., Taoso, M., & Urbano, A. 2017, *Phys. Rev. Lett.*, 119, 031101
 Geballe, T. R. & Oka, T. 2010, *ApJ*, 709, L70
 Ginsburg, A., Henkel, C., Ao, Y., et al. 2016, *A&A*, 586, A50
 Goto, M., Geballe, T. R., Indriolo, N., et al. 2014, *ApJ*, 786, 96
 Goto, M., Usuda, T., Geballe, T. R., et al. 2011, *PASJ*, 63, L13
 H. E. S. S. Collaboration, Abdalla, H., Abramowski, A., et al. 2018, *A&A*, 612, A9
 Henshaw, J. D., Barnes, A. T., Battersby, C., et al. 2023, in *Astronomical Society of the Pacific Conference Series*, Vol. 534, *Protostars and Planets VII*, ed. S. Inutsuka, Y. Aikawa, T. Muto, K. Tomida, & M. Tamura, 83
 HESS Collaboration, Abramowski, A., Aharonian, F., et al. 2016, *Nature*, 531, 476
 Heywood, I., Rammala, I., Camilo, F., et al. 2022, *ApJ*, 925, 165
 Hinton, J. A. & Aharonian, F. A. 2007, *ApJ*, 657, 302
 Indriolo, N. & McCall, B. J. 2012, *ApJ*, 745, 91
 Indriolo, N., Neufeld, D. A., Gerin, M., et al. 2015, *ApJ*, 800, 40
 Jouvin, L., Lemièrre, A., & Terrier, R. 2017, *MNRAS*, 467, 4622

- Kafexhiu, E., Aharonian, F., Taylor, A. M., & Vila, G. S. 2014, *Phys. Rev. D*, 90, 123014
- Khangulyan, D., Aharonian, F. A., & Kelner, S. R. 2014, *ApJ*, 783, 100
- Kissmann, R. 2014, *Astroparticle Physics*, 55, 37
- Krause, J., Morlino, G., & Gabici, S. 2015, in *International Cosmic Ray Conference*, Vol. 34, 34th International Cosmic Ray Conference (ICRC2015), 518
- Kuznetsova, E., Krivonos, R., Lutovinov, A., & Clavel, M. 2022, *MNRAS*, 509, 1605
- LaRosa, T. N., Brogan, C. L., Shore, S. N., et al. 2005, *ApJ*, 626, L23
- Law, C. J., Yusef-Zadeh, F., Cotton, W. D., & Maddalena, R. J. 2008, *ApJS*, 177, 255
- Le Petit, F., Nehmé, C., Le Bourlot, J., & Roueff, E. 2006, *ApJS*, 164, 506
- Le Petit, F., Ruaud, M., Bron, E., et al. 2016, *A&A*, 585, A105
- MAGIC Collaboration, Acciari, V. A., Ansoldi, S., et al. 2020, *A&A*, 642, A190
- McCall, B. J., Huneycutt, A. J., Saykally, R. J., et al. 2003, *Nature*, 422, 500
- McKee, C. F. 1989, *ApJ*, 345, 782
- Miller, S., Tennyson, J., Geballe, T. R., & Stallard, T. 2020, *Reviews of Modern Physics*, 92, 035003
- Neufeld, D. A. & Wolfire, M. G. 2017, *ApJ*, 845, 163
- Oka, T. 2006, *Proceedings of the National Academy of Science*, 103, 12235
- Oka, T., Geballe, T. R., Goto, M., et al. 2019, *ApJ*, 883, 54
- Oka, T., Geballe, T. R., Goto, M., Usuda, T., & McCall, B. J. 2005, *ApJ*, 632, 882
- Orlando, E. 2019, *Phys. Rev. D*, 99, 043007
- Orlando, E. & Strong, A. 2013, *MNRAS*, 436, 2127
- Padovani, M., Galli, D., & Glassgold, A. E. 2009, *A&A*, 501, 619
- Padovani, M., Ivlev, A. V., Galli, D., & Caselli, P. 2018, *A&A*, 614, A111
- Phan, V. H. M., Morlino, G., & Gabici, S. 2018, *MNRAS*, 480, 5167
- Phan, V. H. M., Recchia, S., Mertsch, P., & Gabici, S. 2023, *Phys. Rev. D*, 107, 123006
- Phan, V. H. M., Schulze, F., Mertsch, P., Recchia, S., & Gabici, S. 2021, *Phys. Rev. Lett.*, 127, 141101
- Planck Collaboration, Adam, R., Ade, P. A. R., et al. 2016, *A&A*, 596, A103
- Ponti, G., Hofmann, F., Churazov, E., et al. 2019, *Nature*, 567, 347
- Predehl, P., Sunyaev, R. A., Becker, W., et al. 2020, *Nature*, 588, 227
- Press, W. H., Teukolsky, S. A., Vetterling, W. T., & Flannery, B. P. 1992, *Numerical Recipes in C*, 2nd edn. (Cambridge, USA: Cambridge University Press)
- Recchia, S., Phan, V. H. M., Biswas, S., & Gabici, S. 2019, *MNRAS*, 485, 2276
- Rivilla, V. M., García De La Concepción, J., Jiménez-Serra, I., et al. 2022, *Frontiers in Astronomy and Space Sciences*, 9, 829288
- Sanz-Novo, M., Rivilla, V. M., Jiménez-Serra, I., et al. 2024, *ApJ*, 965, 149
- Sarkar, K. C. 2024, *A&A Rev.*, 32, 1
- Schlickeiser, R. 2002, *Cosmic Ray Astrophysics*
- Strong, A. W., Porter, T. A., Digel, S. W., et al. 2010, *ApJ*, 722, L58
- Su, M., Slatyer, T. R., & Finkbeiner, D. P. 2010, *ApJ*, 724, 1044
- Tatischeff, V., Decourchelle, A., & Maurin, G. 2012, *A&A*, 546, A88
- Terrier, R., Clavel, M., Soldi, S., et al. 2018, *A&A*, 612, A102
- Terrier, R., Ponti, G., Bélanger, G., et al. 2010, *ApJ*, 719, 143
- Thornbury, A. & Drury, L. O. 2014, *MNRAS*, 442, 3010
- Tsuboi, M., Handa, T., & Ukita, N. 1999, *ApJS*, 120, 1
- van der Tak, F. F. S., Belloche, A., Schilke, P., et al. 2006, *A&A*, 454, L99
- Wolfire, M. G., McKee, C. F., Hollenbach, D., & Tielens, A. G. G. M. 2003, *ApJ*, 587, 278
- Yang, R.-z., Li, G.-X., Wilhelmi, E. d. O., et al. 2023, *Nature Astronomy*, 7, 351
- Yusef-Zadeh, F., Hewitt, J. W., Wardle, M., et al. 2013, *ApJ*, 762, 33
- Yusef-Zadeh, F., Muno, M., Wardle, M., & Lis, D. C. 2007, *ApJ*, 656, 847